

# Cathodoluminescence study of disordering of GaAs/AlGaAs quantum wells using an AIAs native oxide and thermal annealing technique

X. Zhang and D. H. Rich<sup>a)</sup>

*Department of Materials Science and Engineering, University of Southern California, Los Angeles, California 90089-0241*

C.-K. Lin and P. D. Dapkus

*Department of Electrical Engineering/ElectroPhysics, University of Southern California, Los Angeles, California 90089-0271*

(Received 26 November 1997; accepted for publication 14 April 1998)

GaAs/AlGaAs quantum wells (QWs), selectively disordered using an AIAs native oxide and thermal annealing technique, were studied using spectrally, spatially, and temporally resolved cathodoluminescence (CL). The spectral shift of the QW luminescence was determined as a function of annealing temperature in the oxide and nonoxide regions. Time-resolved CL was used to assess the impact of defects and the built-in field near the oxide/nonoxide transition region on the carrier lifetime. Spatially resolved CL spectroscopy was used to examine changes in the QW luminescence intensity near the transition region. The carrier lifetime was found to increase in the transition region, owing to the enhanced spatial separation of electrons and holes in this region. From CL images and line scans of three samples annealed at different temperatures, a partial dead region is found between oxide and nonoxide regions. Details of the native oxide formation are discussed.

© 1998 American Institute of Physics. [S0021-8979(98)03514-2]

## I. INTRODUCTION

The native oxide of AIAs has received a great deal of interest recently because of its unique potential to realize complex electronic and optoelectronic device structures.<sup>1-3</sup> Vertical cavity surface emitting lasers employing native oxide current constriction and mode control layers have demonstrated ultralow threshold current laser operation<sup>4-6</sup> and GaAs metal–semiconductor field-effect transistors fabricated on Al<sub>x</sub>O<sub>y</sub> layers have also exhibited excellent performance.<sup>7</sup> A novel impurity-free vacancy diffusion (IFVD) technique using AIAs native oxide as a vacancies source in quantum well (QW) disordering was previously reported, which is believed to have many advantages over the conventional IFVD techniques.<sup>8</sup> In order to further improve this technique, we need to know more about the oxidation process and the subsequent impact of thermal annealing on the optical properties of the GaAs/AlGaAs QWs.

In this article, we report a spatially, spectrally, and temporally resolved cathodoluminescence (CL) study of QW luminescence emitted from regions of varying oxidation and subsequent annealing temperatures. A partial dead-layer region, corresponding to the oxide/nonoxide transition region, was observed and studied with these CL techniques. The luminescence intensity and carrier lifetime were probed with CL in order to assess the impact of the oxide, attendant defects, and built-in field in the oxide/nonoxide transition region on the optical properties. In order to fully evaluate the potential utilization of the selective oxidation approach for current constriction and mode control layers, we must explore the fundamental impact of the oxidation on the optical

properties using a high spatial and spectral resolution optical probe such as in the case of CL, which possesses a spatial resolution of  $\sim 0.5 \mu\text{m}$  for the present material system.

## II. EXPERIMENT

Figures 1(a) and 1(b) show the structure of the sample, which was grown by metal–organic chemical-vapor deposition (MOCVD) on a Si-doped  $n^+$ -GaAs(001) substrate. All the layers shown were undoped. This MOCVD growth procedure is described in detail elsewhere.<sup>8</sup> After the sample was patterned into 500  $\mu\text{m}$  wide stripes with a 50  $\mu\text{m}$  separation using conventional photolithography and wet chemical etching, the wet oxidation was carried out in a 425 °C open quartz tube furnace with 300 sccm ultra-high-purity N<sub>2</sub> bubbled through a 88 °C D.I. water bubbler. About 70  $\mu\text{m}$  wide Al<sub>x</sub>O<sub>y</sub> layers were formed laterally on both sides of the mesas. Three separate samples were then heated to different temperatures in a flowing N<sub>2</sub> atmosphere in a rapid thermal annealer with a ramping rate of  $\sim 1$  °C/s. The temperature was maintained at its maximum for 30 s.

CL experiments were performed with a modified JEOL-840A scanning electron microscope (SEM) using a 15 keV electron beam with a probe current  $I_b$  of 0.6 nA.<sup>9</sup> The luminescence signal was dispersed by a 1/4 m monochromator and detected with a cooled GaAs:Cs photomultiplier tube with a spectral resolution of  $\sim 1$  nm. The temperature of the sample was maintained at  $\sim 87$  K during the CL measurement. Our CL system with time-resolved capability has been described previously<sup>10</sup> and the time-resolved CL experiments were performed with the method of delayed coincidence in an inverted single-photon counting mode, with a time reso-

<sup>a)</sup>Electronic mail: danrich@almaak.usc.edu

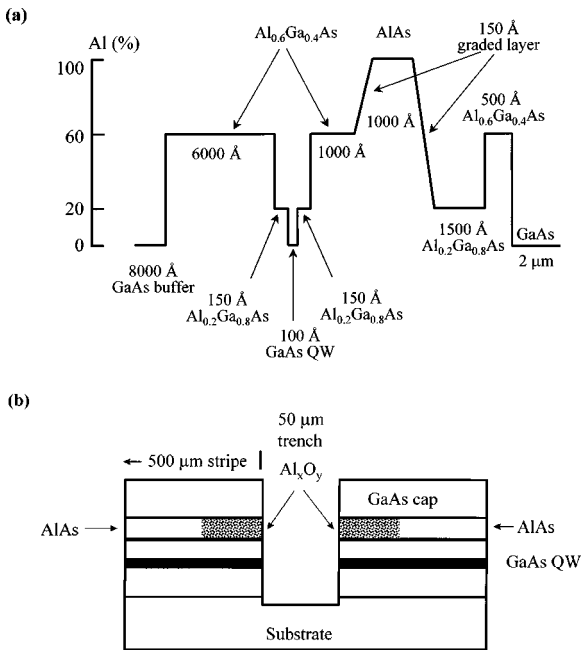


FIG. 1. Schematic of the MOCVD-grown structure for the QW (a) and sample patterning structure (b).

lution of  $\sim 100$  ps.<sup>11</sup> Electron-beam pulses of 50 ns width with a 1 MHz repetition rate were used to excite the samples.

### III. RESULTS AND DISCUSSION

#### A. CL spectroscopy of the oxide-induced disordered GaAs/AlGaAs QW

The GaAs/AlGaAs QW emission peak wavelength shift and CL intensity are shown in Fig. 2 for various annealing temperatures. The QW emission, both in wavelength and intensity, from the nonoxide region changes negligibly for the annealing temperatures shown. We refer to the nonoxide region as also possessing nondisordered QWs since the annealing does not appear to cause interdiffusion of the Al and Ga at the AlGaAs/GaAs QW interfaces. The disordering is likely due to a vacancy-enhanced intermixing of the QW under the native oxide during the rapid thermal annealing.<sup>8</sup> The enhanced QW luminescence intensity for the oxide region as the annealing temperature increases attests to the high structural quality and low defect density of the QWs after annealing. Such an annealing-induced interdiffusion was found to also reduce the interface roughness in the InGaAs/GaAs QW system.<sup>12</sup> Figure 3 shows the local CL spectra taken across the oxide/nonoxide boundary region for the sample annealed at 950 °C. The electron beam is scanned from the oxide region to the nonoxide region over a range of  $\sim 12$  μm. To study the influence of the oxidation front on the optical properties of disordered and nondisordered QWs, we acquired CL spectra near the oxide/nonoxide transition region along an arbitrary line perpendicular to the oxidation front. The e-beam was positioned along this line with steps of 0.13 μm. The boundary of the oxidation front (distance = 0) was determined by the contrast in the conventional secondary electron image of the SEM. The peaks of emission for the disordered and nondisordered QWs are at 765 and

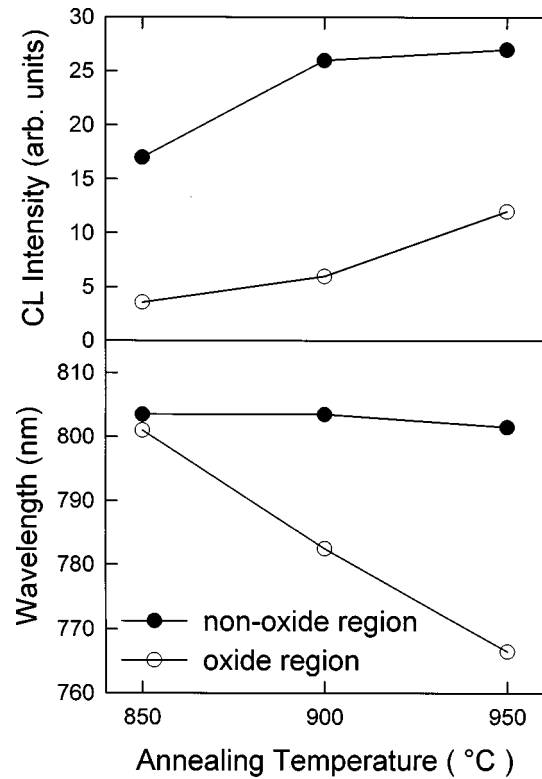


FIG. 2. CL spectroscopy results at  $T=87$  K for QW emission in both the oxide and nonoxide regions. For various end-point annealing temperatures shown, the QW energy shifts were measured with respect to the CL peak wavelength of the as-grown sample. CL peak intensities vs temperatures are also shown.

800 nm, respectively, for the sample annealed at 950 °C. There is a redshift of  $\sim 3$  nm for disordered peaks close to the transition region, indicating the disordering of the QW is slightly reduced at the transition region.

Figure 4 shows the integrated CL intensity over the 750–830 nm spectral range for various e-beam positions relative to the transition region. The data corresponding to the sample of Fig. 3 are labeled as A in Fig. 4. The CL intensity in the oxide region is lower than that in the nonoxide region by a factor of  $\sim 3$ , which can be attributed to (i) reflection losses from native oxide, (ii) an enhanced nonradiative recombination near the oxide layer, and (iii) a reduced diffusive transport of carriers to the QW. The oxide has a significantly lower value of the refractive index than AlAs in the nonoxide region,<sup>13</sup> so an enhanced reflection of the QW luminescence occurs in the oxide region. In order to test the effect of reflection from the oxide, we performed two additional procedures to measure the absolute intensity emitted from the QW. First, we etched away the AlAs and oxide layers after annealing at 950 °C, leaving the  $\sim 1000$  Å of Al<sub>0.6</sub>Ga<sub>0.4</sub>As exposed to the surface and covering the QW. Second, a sample, whose oxidation procedure and annealing temperature of 950 °C were otherwise identical to sample A, was grown with the 1000 Å AlAs region placed below the GaAs QW, opposite to the case illustrated in Fig. 1 for sample A. The samples corresponding to these two procedures are labeled as B and C, respectively, and their integrated CL intensity profile across the oxide/nonoxide transi-

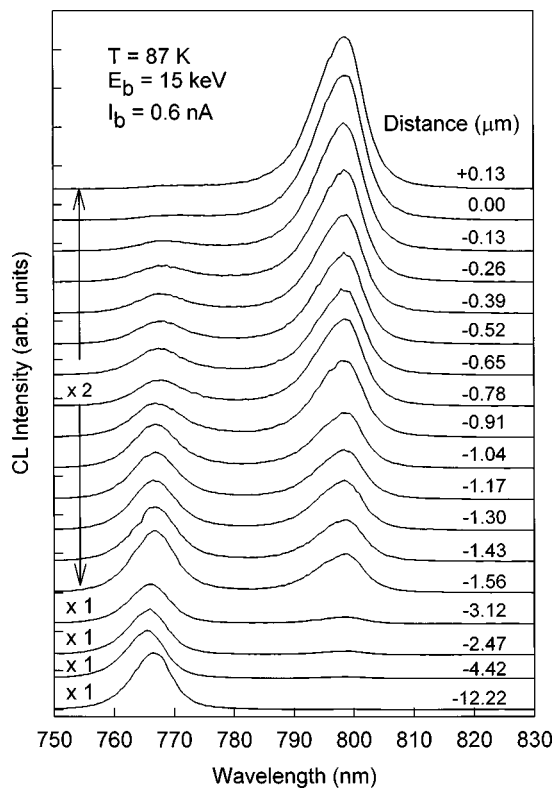


FIG. 3. Local CL spectra acquired along a line perpendicular to the oxide/nonoxide boundary at  $T=87$  K.

tion region is plotted with that of sample A in Fig. 4. We note that the data for samples A and C are offset for clarity in Fig. 4 and are plotted on the same absolute intensity scale as that used for sample B to facilitate a comparison.

It is evident that the position of the oxide, or its absence altogether in sample B, will markedly effect the overall measured CL emission from the oxide region. For sample C, the

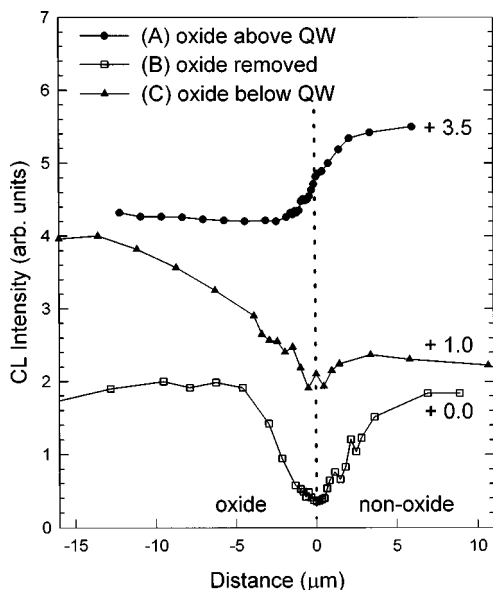


FIG. 4. Absolute CL intensity detected for samples A, B, and C as a function of the distance across the transition region. For clarity, two of the line scans are offset vertically by +3.5 (A) and +1.0 (C).

oxide residing beneath the QW will enhance the luminescence by a factor of  $\sim 1.7$  relative to that for sample B, due to reflection. In samples B and C, the influence of the partial dead region near the oxide/nonoxide transition region on the CL intensity can be seen more clearly without the obstruction of the oxide layer. In sample B, with the oxide layer completely removed, a clear dip in the CL intensity by a factor of  $\sim 4$  is observed relative to positions on both the oxide and nonoxide sides greater than  $\sim 5 \mu\text{m}$  from the boundary (distance=0). Further, the nearly identical integrated CL intensities in the oxide and nonoxide regions of sample B for distances greater than  $\sim 5 \mu\text{m}$  from the transition region is also evidence that the vacancy-induced disorder of the QW does not seriously degrade the optical properties of the disordered QW. Thus, the placement of the oxide will significantly influence the absolute luminescence detected from the oxide and nonoxide regions. The removal of the oxide permits a meaningful comparison of the integrated CL emission from both the disordered and nondisordered QWs.

It is significant to note that there is both nondisordered and disordered QW peaks for e-beam positions in the oxide region more than  $3 \mu\text{m}$  away from boundary of the oxide and nonoxide regions, as observed in Fig. 3. The simplest interpretation is that carriers drift from the higher QW band-gap region in the oxide region to the lower QW band-gap region in the nonoxide region, owing to the built-in electric field. The built-in field causes carriers, which are generated in the lower QW band-gap region of the nonoxide near the boundary, to be repelled from the higher QW band-gap region of the oxide. Furthermore, this carrier drift results in a full width at half maximum (FWHM) of  $\sim 6 \mu\text{m}$  for the dip in the intensity data for sample B of Fig. 4. The FWHM is considerably greater than the minority-carrier diffusion length of  $\sim 1 \mu\text{m}$ , owing to the presence of the built-in field.

### B. Monochromatic CL imaging of the transition region between disordered and ordered QWs

The usefulness of the disordering technique in achieving a lateral spatial confinement or restriction of carriers may strongly depend on the sharpness of the transition region. Monochromatic CL images were taken over a  $43 \mu\text{m} \times 31 \mu\text{m}$  region with QW emission wavelengths corresponding to the nonoxide region (800 nm) and oxide region (765 nm), as shown in Fig. 5. The CL images of the oxide and nonoxide regions are smooth and homogeneous away from the transition region. However, the transition region in Fig. 5(a) is not sharp and smooth as many protrusions are seen along the transition edge. A composite image is formed by summing pixel intensity values in Figs. 5(a) and 5(b) and shown in Fig. 5(c). The partial dead layer, whose width and contrast varies along the boundary edge, is clearly observed in the image. Also shown in Fig. 5(c) is a line along which the local spectra of Fig. 3 were acquired.

To examine the dark gap regions, local CL spectra were further acquired at points *P*, *Q*, and *R* marked in Fig. 5(c) and plotted in Fig. 6. Spectra *P* and *Q* were taken in the dark region, with spectrum *P* closer to the oxide region. Spectrum *R* was taken in the nonoxide region far away from the tran-

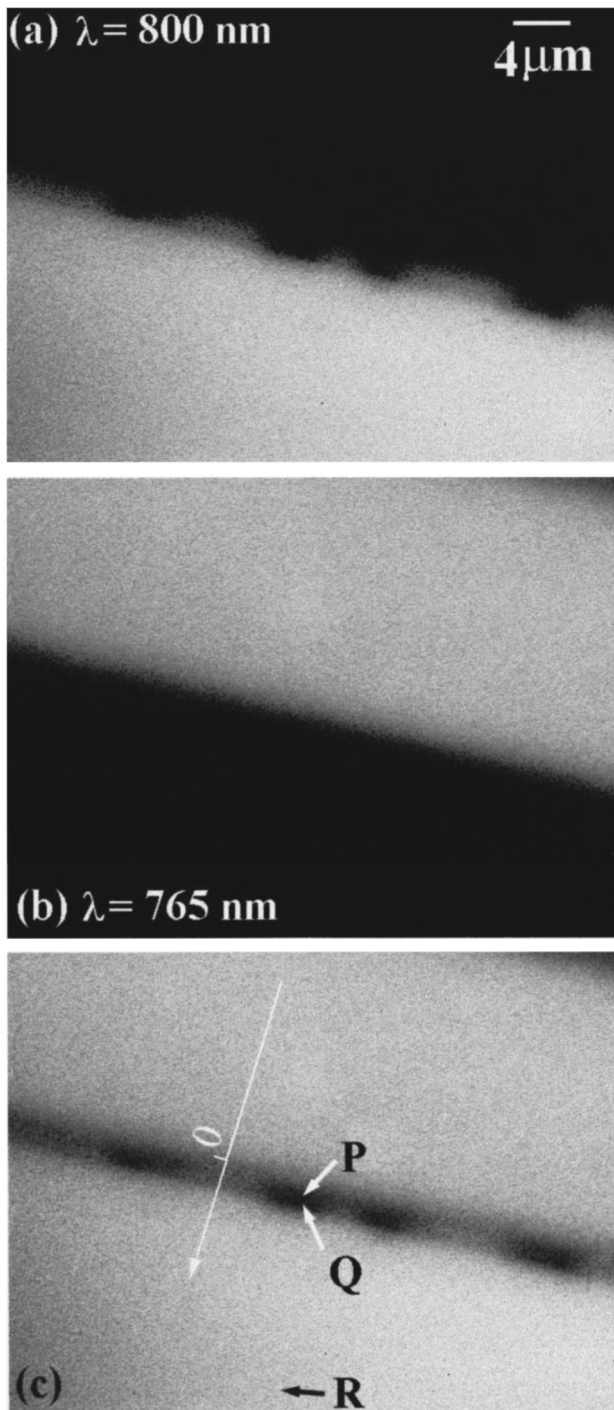


FIG. 5. Monochromatic CL images of QW emission in the nonoxide region (a), QW emission in the oxide region (b), and a composite image (c) that was obtained by summing pixels in (a) and (b).

sition region as a reference. The 765 nm peak corresponding to the disordered QW was not observed in the dark gap region. We conclude that (i) the built-in field arising from the spatial variation in the QW band gap is sufficiently strong in the dark regions to prevent carriers from recombining in the disordered QW region, and (ii) the transition from the ordered to the disordered QW regions is abrupt ( $\ll 0.5 \mu\text{m}$ ) as also evidenced by the appearance of only two peaks in the QW spectra of Fig. 3.

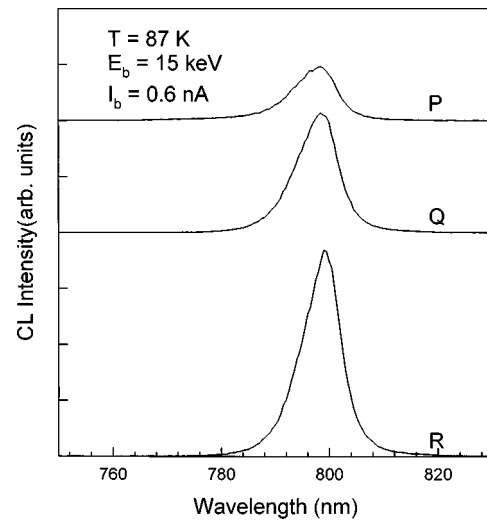


FIG. 6. Local CL spectra taken in the dark gap region of Fig. 4(c). Spectra P and Q were acquired in the dark gap region, as shown in Fig. 5(c), and R was taken in the nonoxide region far from the transition region.

Figure 7 shows monochromatic CL images of 800 nm emission wavelength of three samples having the structure of Fig. 1 and annealed at different temperatures of 850, 900, and 950 °C. The transition boundary is quite smooth and sharp for the sample annealed at 850 °C. As the annealing temperature is increased from 900 to 950 °C, the protrusions and nonuniformity at the transition edge become more pronounced. Thus, the nonuniformity at the transition edge is directly related to the annealing temperature. The higher temperature anneal of 950 °C appears to activate the oxidation front, causing a spreading of the oxidation further into the nonoxide regions. This spreading, while nonuniform, does not appear to influence the interdiffusion of Al and Ga at the AlGaAs/QW interface, as only two QW peaks were observed in Fig. 3.

### C. Time-resolved CL analysis of recombination near the oxide/nonoxide transition region

Time-resolved CL transients of the CL intensity decay versus time were acquired at various positions relative to the transition region for both the disordered and nondisordered QW emissions. Four transients are shown in Fig. 8 with the corresponding emission wavelengths and e-beam position relative to the transition region. In order to obtain a lifetime for each decay curve, the initial decay was fit with an exponential with a constant lifetime, as shown in the semilog plot of Fig. 8. Deviations from the simple exponential rate law at long times are expected due to the presence of additional defect- and impurity-related recombination channels.<sup>11</sup> A plot of the lifetime versus e-beam position (distance) is shown in Fig. 9 for the emissions from the disordered (766 nm) and the nondisordered (800 nm) QWs.

The lifetimes for the disordered and nondisordered QW luminescence are 1.3 and 1.6 ns, respectively, far from the oxide/nonoxide boundary (distance=0). The reduced lifetime in the oxide region containing the disordered QW is likely due to the enhanced defect density, largely caused by the oxide-enhanced vacancy diffusion. Additional recombi-

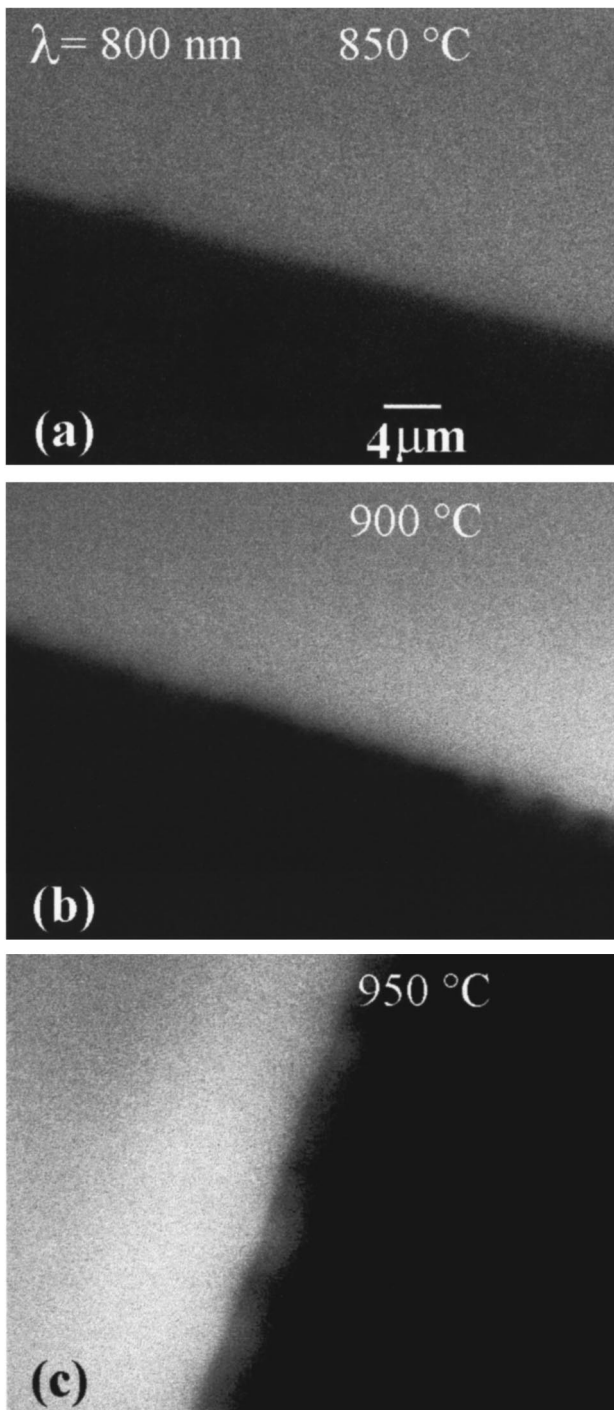


FIG. 7. Monochromatic CL images of the QW emission in the nonoxide region for three samples with 850, 900, and 950 °C end-point annealing temperatures in (a), (b), and (c), respectively.

nation centers are expected to reduce the average carrier lifetime. As the e-beam is placed close to the transition region, the lifetime for both types of QWs increases. The increased lifetime for the disordered QW (766 nm) for distances between 0 and  $-6 \mu\text{m}$  may be due to a reduced defect density in this region, as it is closer to the nonoxide region. Likewise, the reduced CL intensity near the transition region (Fig. 4) is also consistent with a reduced radiative recombination rate and longer lifetime in the absence of additional

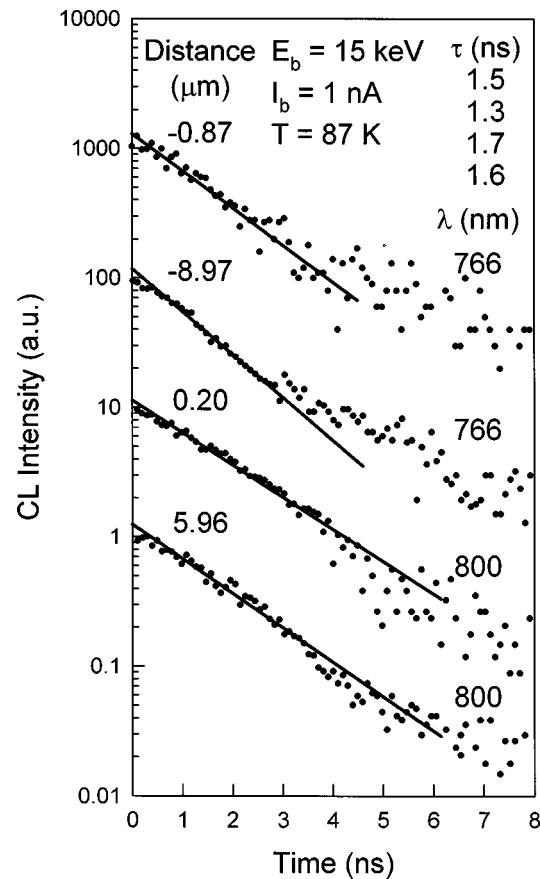


FIG. 8. CL transients for 800 and 766 nm peaks at different positions relative to the oxide/nonoxide transition region.

defect-related nonradiative recombination centers in this region. We suggest that the increased lifetime is caused by the built-in field. A small field-induced separation of electrons and holes will likely lead to an increased excitonic recombination lifetime.<sup>14</sup> An increase in lifetime for emission from the ordered QW (800 nm) is also observed in the 0– $\sim 3 \mu\text{m}$  range on the nonoxide side of the transition region, which is also likely caused by the field. However, there is a sudden drop in the lifetime from 1.7 to 1.3 ns for emission from the ordered QW for e-beam positions just crossing into the oxide region (0 to  $-2 \mu\text{m}$ ). In this region, generated electrons and holes are subject to a higher defect density.

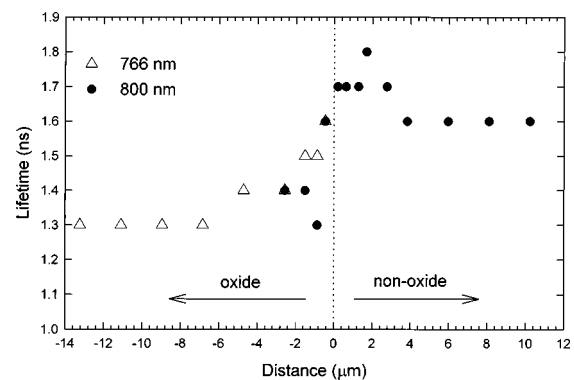


FIG. 9. Lifetime vs e-beam positions for both the disordered and nondisordered QW emission.

Those carriers which drift back into the nonoxide region can also recombine through defect-related nonradiative recombination channels in the oxide region, in addition to the radiative channel of the ordered QW in the nonoxide region. This competition will, therefore, reduce the average lifetime for the nondisordered QW emission (800 nm) in the 0 to  $-2 \mu\text{m}$  range. Thus, the asymmetry in the lifetime profile of Fig. 9 for the ordered and nondisordered QW emissions is explained by a combination of vacancy defects and the presence of a built-in field.

#### IV. CONCLUSION

In conclusion, we have examined the interdiffusion and disordering of AlGaAs/GaAs QWs using wet oxidation and thermal annealing. The CL spectroscopy and imaging was employed to study the uniformity of the QWs in the oxide and nonoxide regions and the transition region. Monochromatic CL images of the QW emission in both oxide and nonoxide regions exhibit a dark gap region, indicative of the dead layer that forms from the lateral built-in field in the transition region. Etching and removal of the oxide region revealed that disordering of the QW did not measurably degrade its optical quality in luminescence. Time-resolved CL was used to assess the impact of the built-in field on the luminescence lifetime. Spatially resolved lifetime measurements determined that the lifetime increases near the transition region, owing to the enhanced spatial separation of electrons and holes in this region. The annealing temperature was found to influence the uniformity of the transition region, and higher annealing temperatures resulted in an enhanced nonuniformity. Eventually, we anticipate that these

results will impact the choice of device patterning designs and processing conditions for devices relying on sub- $\mu\text{m}$  current constriction.

#### ACKNOWLEDGMENTS

This work was supported by the U.S. Army Research Office and the National Science Foundation.

- <sup>1</sup>S. Guha, F. Agahi, B. Pezeshki, J. A. Kash, D. W. Kisker, and N. A. Bojarczuk, *Appl. Phys. Lett.* **68**, 906 (1996).
- <sup>2</sup>R. D. Twisten, D. M. Follstaedt, K. D. Choquette, and R. P. Schneider, Jr., *Appl. Phys. Lett.* **69**, 19 (1997).
- <sup>3</sup>C. I. H. Ashby, J. P. Sullivan, P. P. Newcomer, N. A. Missert, H. Q. Hou, B. E. Hammons, M. J. Hafich, and A. G. Baca, *Appl. Phys. Lett.* **70**, 2443 (1997).
- <sup>4</sup>D. L. Huffaker, D. G. Deppe, K. Kumar, and T. J. Rogers, *Appl. Phys. Lett.* **65**, 97 (1994).
- <sup>5</sup>K. D. Choquette, R. P. Schneider, Jr., K. L. Lear, and K. M. Geib, *Electron. Lett.* **65**, 97 (1994).
- <sup>6</sup>G. M. Yang, M. H. MacDougal, and P. D. Dapkus, *Electron. Lett.* **31**, 886 (1995).
- <sup>7</sup>A. E. Bond, C.-K. Lin, M. H. Macdougall, P. D. Dapkus, K. Kaviani, O. Adamczyk, and R. Nottenburg, *Electron. Lett.* **32**, 2271 (1996).
- <sup>8</sup>C.-K. Lin, X. Zhang, P. D. Dapkus, and D. H. Rich, *Appl. Phys. Lett.*, **71**, 3108 (1997).
- <sup>9</sup>D. H. Rich, A. Ksendzov, R. W. Terhune, F. J. Grunthaner, B. A. Wilson, H. Shen, M. Dutta, S. M. Vernon, and T. M. Dixon, *Phys. Rev. B* **43**, 6836 (1991).
- <sup>10</sup>H. T. Lin, D. H. Rich, A. Konkar, P. Chen, and A. Madhukar, *J. Appl. Phys.* **81**, 3186 (1997).
- <sup>11</sup>D. Bimberg, H. Münzel, A. Steckenborn, and J. Christen, *Phys. Rev. B* **31**, 7788 (1985).
- <sup>12</sup>K. Rammohan, D. H. Rich, M. H. MacDougal, and P. D. Dapkus, *Appl. Phys. Lett.* **70**, 1599 (1997).
- <sup>13</sup>The values of the refractive index  $n$  for AlAs,  $\text{Al}_2\text{O}_3$ , and GaAs are 2.86, 1.76, and 3.32, respectively; see, e.g., M. Bass *et al.*, in *Handbooks of Optics II*, 2nd ed. (McGraw-Hill, New York, 1995), pp. 33 and 56.
- <sup>14</sup>D. H. Rich, H. T. Lin, and A. Larsson, *J. Appl. Phys.* **77**, 6557 (1995).